Compact silicon photonic waveguide modulator based on the vanadium dioxide metal-insulator phase transition

Ryan M. Briggs,[1,*] Imogen M. Pryce,[1] and Harry A. Atwater[1,2]

[1]*Thomas J. Watson Laboratories of Applied Physics, California Institute of Technology, Pasadena, CA 91125, USA*
[2]*Kavli Nanoscience Institute, California Institute of Technology, Pasadena, CA 91125, USA*
**rbriggs@caltech.edu*

Abstract: We have integrated lithographically patterned VO_2 thin films grown by pulsed laser deposition with silicon-on-insulator photonic waveguides to demonstrate a compact in-line absorption modulator for use in photonic circuits. Using single-mode waveguides at λ = 1550 nm, we show optical modulation of the guided transverse-electric mode of more than 6.5 dB with 2 dB insertion loss over a 2-μm active device length. Loss is determined for devices fabricated on waveguide ring resonators by measuring the resonator spectral response, and a sharp decrease in resonator quality factor is observed above 70 °C, consistent with switching of VO_2 to its metallic phase. A computational study of device geometry is also presented, and we show that it is possible to more than double the modulation depth with modified device structures.

OCIS codes: (130.3120) Integrated optics devices; (130.4110) Modulators; (160.6840) Thermo-optical materials; (230.5750) Resonators; (230.7380) Waveguides, channeled.

References and links

1. F. J. Morin, "Oxides which show a metal-to-insulator transition at the Neel temperature," Phys. Rev. Lett. **3**(1), 34–36 (1959).
2. J. B. Goodenough, "The two components of crystallographic transition in VO_2," J. Solid State Chem. **3**(4), 490–500 (1971).
3. A. Cavalleri, C. Tóth, C. W. Siders, J. A. Squier, F. Ráksi, P. Forget, and J. C. Kieffer, "Femtosecond structural dynamics in VO_2 during an ultrafast solid-solid phase transition," Phys. Rev. Lett. **87**(23), 237401 (2001).
4. H. T. Kim, Y. W. Lee, B. J. Kim, B. G. Chae, S. J. Yun, K. Y. Kang, K. J. Han, K. J. Yee, and Y. S. Lim, "Monoclinic and correlated metal phase in $VO_{(2)}$ as evidence of the Mott transition: coherent phonon analysis," Phys. Rev. Lett. **97**(26), 266401 (2006).
5. B. G. Chae, H. T. Kim, D. H. Youn, and K. Y. Kang, "Abrupt metal–insulator transition observed in VO_2 thin films induced by a switching voltage pulse," Physica B **369**(1-4), 76–80 (2005).
6. C. Ko, and S. Ramanathan, "Observation of electric field-assisted phase transition in thin film vanadium oxide in a metal-oxide-semiconductor device geometry," Appl. Phys. Lett. **93**(25), 252101 (2008).
7. S. Chen, X. Yi, H. Ma, H. Wang, X. Tao, M. Chen, and C. Ke, "A novel structural VO_2 micro-optical switch," Opt. Quantum Electron. **35**(15), 1351–1355 (2003).
8. L. Jiang, and W. N. Carr, "Design, fabrication and testing of a micromachined thermo-optical light modulator based on a vanadium dioxide array," J. Micromech. Microeng. **14**(7), 833–840 (2004).
9. Q. Xu, B. Schmidt, S. Pradhan, and M. Lipson, "Micrometre-scale silicon electro-optic modulator," Nature **435**(7040), 325–327 (2005).
10. A. Liu, R. Jones, L. Liao, D. Samara-Rubio, D. Rubin, O. Cohen, R. Nicolaescu, and M. Paniccia, "A high-speed silicon optical modulator based on a metal-oxide-semiconductor capacitor," Nature **427**(6975), 615–618 (2004).
11. E. L. Wooten, K. M. Kissa, A. Yi-Yan, E. J. Murphy, D. A. Lafaw, P. F. Hallemeier, D. Maack, D. V. Attanasio, D. J. Fritz, G. J. McBrien, and D. E. Bossi, "A review of lithium niobate modulators for fiber-optic communications system," IEEE J. Sel. Top. Quantum Electron. **6**(1), 69–82 (2000).
12. T. Ido, S. Tanaka, M. Suzuki, M. Koizumi, H. Sano, and H. Inoue, "Ultra-high-speed multiple-quantum-well electro-absorption optical modulators with integrated waveguides," J. Lightwave Technol. **14**(9), 2026–2034 (1996).
13. G. Gopalakrishnan, D. Ruzmetov, and S. Ramanathan, "On the triggering mechanism for the metal-insulator transition in thin film VO_2 devices: electric field versus thermal effects," J. Mater. Sci. **44**(19), 5345–5353 (2009).
14. G. Stefanovich, A. Pergament, and D. Stefanovich, "Electrical switching and Mott transition in VO_2," J. Phys. Condens. Matter **12**(41), 8837–8845 (2000).

#125843 - $15.00 USD Received 23 Mar 2010; revised 29 Apr 2010; accepted 4 May 2010; published 12 May 2010

15. M. A. Webster, R. M. Pafchek, A. Mitchell, and T. L. Koch, "Width dependence of inherent TM-mode lateral leakage loss in silicon-on-insulator ridge waveguides," IEEE Photon. Technol. Lett. **19**(6), 429–431 (2007).
16. R. M. Briggs, M. Shearn, A. Scherer, and H. A. Atwater, "Wafer-bonded single-crystal silicon slot waveguides and ring resonators," Appl. Phys. Lett. **94**(2), 021106 (2009).
17. J. Y. Suh, R. Lopez, L. C. Feldman, and R. F. Haglund, Jr., "Semiconductor to metal phase transition in the nucleation and growth of VO_2 nanoparticles and thin films," J. Appl. Phys. **96**(2), 1209–1213 (2004).
18. L. J. van der Pauw, "A new method of measuring the resistivity and Hall coefficients on lamellae of arbitrary shape," Philips Tech. Rev. **20**, 220–224 (1958).
19. K. Preston, and M. Lipson, "Slot waveguides with polycrystalline silicon for electrical injection," Opt. Express **17**(3), 1527–1534 (2009).
20. R. A. Soref, and B. R. Bennett, "Electrooptical effects in silicon," IEEE J. Quantum Electron. **23**(1), 123–129 (1987).
21. M. Borselli, T. J. Johnson, and O. Painter, "Beyond the Rayleigh scattering limit in high-Q silicon microdisks: theory and experiment," Opt. Express **13**(5), 1515–1522 (2005).
22. J. A. McCaulley, V. M. Donnelly, M. Vernon, and I. Taha, "Temperature dependence of the near-infrared refractive index of silicon gallium arsenide, and indium phosphide," Phys. Rev. B **49**(11), 7408–7417 (1994).
23. H. S. Choi, J. S. Ahn, J. H. Jung, T. W. Noh, and D. H. Kim, "Mid-infrared properties of a VO_2 film near the metal-insulator transition," Phys. Rev. B **54**(7), 4621–4628 (1996).

1. Introduction

The thermochromic phase transition of crystalline VO_2 occurring near 68 °C [1] has been of interest in recent years for its potential applications in active optical devices. Monophase VO_2 can be transformed from a relatively transparent insulating state with monoclinic crystal structure to a metallic rutile phase upon application of thermal [2], optical [3,4], or electrical [5,6] stimuli. The phase transition has been reported to occur on a time scale of 10^{-8} s under an applied electric field or by direct heating [5,7] and down to 10^{-13} s using ultrafast optical pumping [3]. Furthermore, recent evidence suggests that the change in electronic properties can be induced independent of a structural transition [4,5], explaining the surprisingly short switching times observed by optical pumping, and suggesting that similarly short transitions might be achieved using an externally gated electric field. When switched by direct thermal stimulus, the rate of switching back to the insulating phase can be quite slow and depends on the thermal properties of a particular device; however, optically and electrically switched VO_2 films have been reported to regain their insulating-phase properties over time scales on the order of 10^{-8} s [3,5]. To date, there have been demonstrations of VO_2-based free-space optical modulators at infrared [7] and visible [8] wavelengths, where local heating was employed to induce the VO_2 phase transition. While these studies show promising results, many of the potential applications of a modulator operating at telecommunications wavelengths require compact integration of waveguide-coupled devices on a Si chip.

Several Si-based waveguide modulator designs have been investigated to compete with more conventional III-V and $LiNbO_3$-based modulators. Prime examples of this technology take advantage of small changes in the refractive index of Si due to voltage-induced variations in charge density. When integrated with a high-quality cavity [9] or Mach-Zehnder interferometer (MZI) [10], such perturbations of the index can result in greater than 15 dB modulation of a single wavelength with modulation frequencies in excess of 1 GHz; however, in order to accommodate interferometric structures, these devices have linear dimensions greater than 10 μm and are limited to a narrow spectral range. In comparison, $LiNbO_3$-based modulators can produce greater than 20 dB modulation at frequencies above 10 GHz [11], but they often employ MZI schemes and are relatively large. Compound-semiconductor electro-absorption waveguide modulators have been shown to be competitive with $LiNbO_3$ devices and have the advantage of broader wavelength operation; however, such devices often require propagation distances on the order of 100 μm [12] due to limited absorption modulation and modal overlap.

Future scalable optical modulator designs are expected to operate with switching energies on the order of 10^{-15} J. For small volumes and short time scales, the thermal energy density required to induce the VO_2 phase transition in a thermally isolated device is approximately $c_p \rho \Delta T$, where c_p = 690 J/(kg K) is the heat capacity of insulating VO_2, $\rho = 4.3\times10^{-3}$ kg/cm^3 is the material density, and ΔT is the required temperature increase [13,14]. For a device

#125843 - $15.00 USD Received 23 Mar 2010; revised 29 Apr 2010; accepted 4 May 2010; published 12 May 2010

initially at room temperature, this energy density is ~10^2 J/cm^3, and a typical thin film device with a thickness of less than 100 nm and a footprint of 1 μm^2 will have a switching energy on the order of 10^{-11} J. In comparison, for electrically driven VO_2 devices with switching times on the order of 10^{-8} s, the field required to induce the VO_2 phase transition has been reported to be ~10^5 V/cm [6], and the leakage current at the transition is ~10^4 A/cm^2 [5,13]. The corresponding switching energy for the previously mentioned device geometry is 10^{-12} J, indicating that athermal switching can potentially be more efficient than thermal switching. To achieve even lower switching energies, it is feasible to envision device designs that, for example, further decrease the required volume of VO_2 or reduce the leakage current through a VO_2 film while still achieving the critical electric field required for the phase transformation.

The dramatic changes in absorption associated with the VO_2 transition, combined with the possibility of ultrafast modulation, make VO_2 an attractive candidate for the next generation of active integrated optical components suitable for broadband applications. As a step toward integrating VO_2-based devices into a Si photonics platform, we have fabricated compact, lithographically defined VO_2 modulators on silicon-on-insulator (SOI). We use substrate heating to thermally induce the VO_2 phase transition, and by demonstrating the efficacy of these devices as integrated absorption modulators, we intend to motivate future work to develop devices that operate on fundamentally faster time scales using localized electrical or optical stimuli. For a modulator with an active device length of 2 μm, we observe thermally induced optical modulation of a confined waveguide mode in excess of 6.5 dB at λ = 1550 nm, with 2 dB insertion loss. A 16-fold increase in VO_2 absorption across the phase transition allows the modulator to function as an effective single-pass device that is compact and broadband, in contrast to MZI and resonator-based designs. Electromagnetic simulations indicate that even deeper modulation is possible with modified device geometries. We also show that waveguide-based devices can be used to probe fundamental phase transition properties, including hysteresis and the insulator-to-metal percolation threshold.

2. Device fabrication

To measure the optical loss induced by integrated VO_2 modulator devices, we first fabricated SOI test bed structures consisting of through-port waveguides evanescently coupled to large-diameter ring resonators, as shown in Fig. 1. The resonators are not a fundamental component of the modulator design, but they facilitate loss measurements independent of temperature-related changes in the amount of optical power coupled into the SOI waveguides. We used SOI with a lightly doped *p*-type (~10^{15} cm^{-3}) 220-nm Si device layer on a 3-μm buried oxide, and patterns were defined using Micro Resist Technology ma-N 2403 resist with high-resolution electron-beam exposure. A waveguide width of 720 nm was chosen so that only the fundamental transverse-electric (TE) and transverse-magnetic (TM) modes are supported at λ = 1550 nm, while minimizing leakage loss from the TM mode [15]. To couple light into and out of the through-port waveguides, we defined symmetrical pairs of 30 μm-wide, 50 μm-long diffraction gratings with a 685-nm pitch, connected to linear waveguide sections via 500 μm linear tapers [16]. Finally, 400 μm-diameter rings, which exhibit negligible bending loss, were patterned alongside the through-port waveguides, with a 1-μm coupling gap.

The waveguide pattern was transferred into the SOI to a depth of 40 nm using a C_4F_8/O_2 plasma etching process in an Oxford Instruments ICP 380 system. The resist was removed along with residual polymer etch products in a 3:1 Piranha solution of H_2SO_4 and 30% H_2O_2 at 100 °C. After cleaning in buffered HF, the resonators were characterized using a fiber-coupled New Focus 6428 Vidia Swept tunable diode laser in order to obtain a baseline measurement of the ring resonator quality factor. Light was delivered to and extracted from the gratings using lensed fiber focusers, and waveguide modes of different polarization were accessed selectively by setting the input polarization and the coupling angle, as described in Ref. 16. Through-port transmission was measured with a fiber-coupled InGaAs photoreceiver that has nearly uniform response across the wavelength range of interest in this work.

After optical characterization, the native oxide was removed from the waveguides with another HF dip, and samples were immediately inserted into a vacuum chamber for pulsed-

#125843 - $15.00 USD Received 23 Mar 2010; revised 29 Apr 2010; accepted 4 May 2010; published 12 May 2010

laser deposition of VO_2. Samples were heated to 500 °C, and deposition was performed by ablating a vanadium metal target with 300-mJ pulses from an excimer laser at a rate of 10 Hz in 12 mTorr O_2. For the devices considered here, VO_2 layers were deposited to an average thickness of 65 nm, which was verified by atomic force microscopy (AFM). To pattern the VO_2 tabs, waveguide samples were again coated with resist, and tabs were patterned by electron beam lithography. The pattern was transferred into the VO_2 using Cr etchant (dilute $(NH_4)_2Ce(NO_3)_6$ and $HClO_4$), and the resist was removed in acetone. All VO_2 was removed from control resonators, which were tested again in the coupling setup described above to verify that resonator quality factor was not impacted by VO_2 deposition and etching.

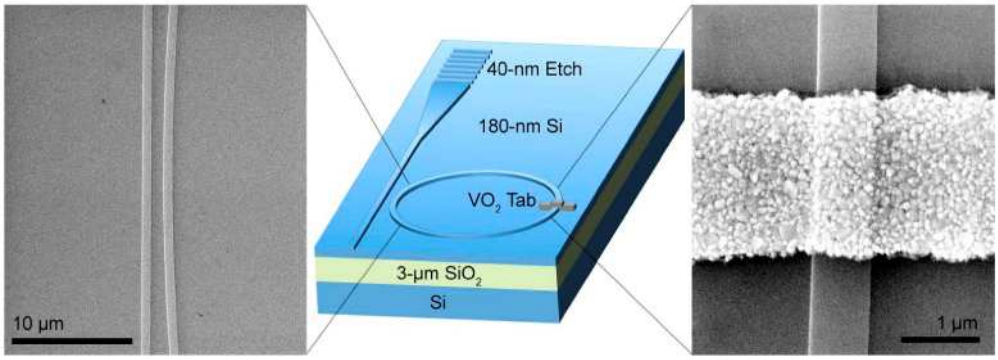

Fig. 1. Schematic of the VO_2 modulator test bed, with a grating-coupled through-port waveguide and an evanescently coupled ring resonator. The scanning electron micrographs show the 1-μm coupling gap between the through-port waveguide and the 400 μm-diameter ring resonator (left) and a lithographically defined 2 μm-long polycrystalline VO_2 tab (right).

3. VO_2 characterization

In order to characterize the VO_2 on the SOI test bed structures, thin films were deposited simultaneously on high-resistivity Si(001) substrates and analyzed by multiple-angle spectroscopic ellipsometry in the near-infrared and X-ray diffractometry (XRD). Figure 2(a) shows the real and imaginary parts of the index of refraction, *n* and *k*, of a 65-nm VO_2 film, as extracted from the ellipsometry amplitude and polarization parameters, Ψ and Δ. Three sets of Ψ and Δ spectra were collected at reflection angles of 60°, 65°, and 70° from the surface normal. To obtain the complex index, the VO_2 film was modeled as a dispersionless but lossy material over a wavelength window of 50 nm. With the thickness fixed at the value measured by AFM, the values of *n* and *k* were adjusted by a minimization algorithm to achieve the smallest error between the modeled and measured values of Ψ and Δ at all three angles simultaneously. The fitting process was repeated as the 50-nm wavelength window was moved along the measured spectrum in increments of 10 nm. The resulting discrete *n* and *k* values are plotted in Fig. 2(a) along with the polynomial fits used in the simulations described in Section 5. This interval fitting method functions as a running average filter to reduce noise in the extracted index values, and it allows for material dispersion to be determined without a phenomenological model of the material's optical properties. The method is acceptable for both phases of VO_2 in the near infrared since the index varies slowly with wavelength.

#125843 - $15.00 USD Received 23 Mar 2010; revised 29 Apr 2010; accepted 4 May 2010; published 12 May 2010

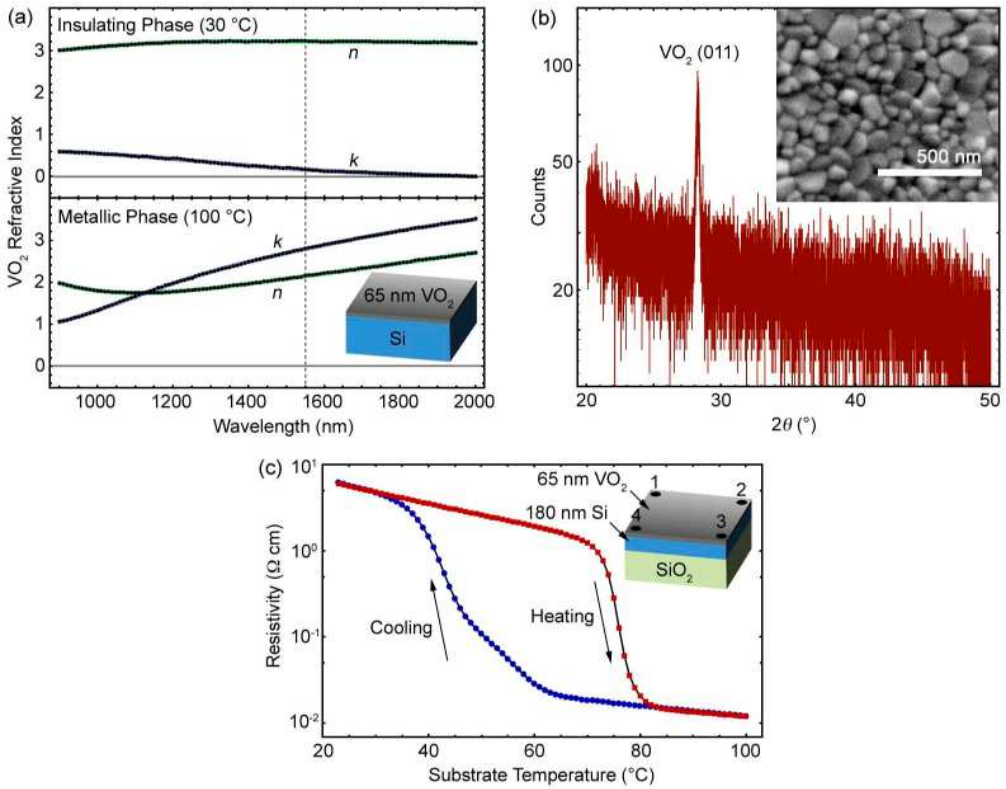

Fig. 2. (a) Real, n, and imaginary, k, parts of the index of refraction of a 65 nm-thick VO_2 film on Si measured by multiple-angle spectroscopic ellipsometry across the near infrared spectrum. (b) X-ray diffraction spectrum of the same polycrystalline VO_2 film (scanning electron micrograph shown in inset). (c) Electrical resistivity versus temperature of a 65 nm-thick VO_2 film on SOI measured using the four-point van der Pauw method.

At 1550 nm, the index of VO_2 is $3.21 + 0.17i$ near room temperature and $2.15 + 2.79i$ when heated to 100 °C, which indicates a clear transition from a nearly transparent state to a phase with metallic optical properties. In particular, the more than 16-fold increase in absorption is the basis for our optical modulator. Also, the optical properties for each phase are nearly constant over the telecommunications C-band (1530 to 1565 nm), making VO_2 a suitable material for broadband devices.

As shown in Fig. 2(b), the XRD spectrum of the same 65-nm VO_2 film produces a strong peak near 28°, corresponding to the (011) plane of VO_2. The spectrum is absent any peaks related to other stoichiometries of vanadium oxide, indicating single-phase crystalline growth. The scanning electron micrograph in the inset of Fig. 2(b) shows an average crystal grain size of nearly 100 nm. In terms of crystallinity and morphology, our films resemble those deposited at low temperature and subsequently oxidized at 450 °C [17], indicating that our *in situ* oxidation process is comparably effective at producing monophase VO_2 on Si.

Finally, we measured the electrical resistivity of the VO_2 film on a small chip of SOI using the four-point van der Pauw method [18]. The temperature was changed in increments of 1 °C at a rate of less than 1 °C/min, and the resistivity was measured for all the various source-probe configurations possible with four symmetric points. At each temperature, all resistivity measurements agreed to within 5%, and the averaged values of resistivity are plotted in Fig. 2(c). Near room temperature, the measured resistivity is nearly equal to that of the top Si layer alone, indicating that the VO_2 is not significantly more conductive than lightly doped Si; however, upon heating above 70 °C, we observe an abrupt transition to the much more conductive metallic phase. Upon cooling, the film regains its insulating-phase properties, but

#125843 - $15.00 USD Received 23 Mar 2010; revised 29 Apr 2010; accepted 4 May 2010; published 12 May 2010

with a much less abrupt transition with respect to temperature. In particular, the VO_2 does not completely switch back to its insulating phase until it has cooled to nearly 40 °C. This broad hysteresis is expected for films with the microstructure observed here, as previously reported by Suh, *et al.* [17].

4. Modulator performance

We probed the loss induced by waveguide-integrated VO_2 tabs by measuring the linewidth of TE-polarized whispering-gallery mode resonances of the SOI test bed structures. Here, we define TE modes as those with the dominant orientation of the electric field parallel to the top waveguide surface. Using the coupling setup described in Section 2, laser radiation near 1550 nm was coupled via surface relief gratings into the through-port waveguides. Maximum coupling efficiency was achieved for an angle of 30° between the waveguide surface normal and the optical axis of the fiber focusers [16]. Through-port transmission was measured as the input wavelength was swept from 1550 to 1551 nm at 1 nm/s. This wavelength range was always sufficient to capture at least one resonance, since the free-spectral range (FSR) of modes of adjacent azimuthal order for our ring resonator geometry is approximately 0.5 nm.

As a baseline reference, the through-port transmission for a bare 400 μm-diameter ring resonator from which all VO_2 was removed is shown in Fig. 3(a). At 30 °C, the resonance at $\lambda_0 = 1550.706$ nm has a linewidth, $\delta\lambda$, of 14.1 pm and a FSR, $\Delta\lambda$, of 0.510 nm. By the relation $Q = \lambda_0/\delta\lambda$ (valid for $\delta\lambda << \lambda_0$), this corresponds to a loaded quality factor $Q_{ref} = 110{,}000$. For $\Delta\lambda << \lambda_0$, the group index is approximately $n_g = \lambda_0^2/(\Delta\lambda L) = 3.75$, where $L = 400\pi$ μm is the round-trip length of the ring resonator. By fitting the Lorentzian lineshape of the through-port transmission, T, to the function [19]

$$T(\lambda) = \frac{(a-r)^2 + (2\pi n_g L)^2 ra\dfrac{(\lambda-\lambda_0)^2}{\lambda_0^4}}{(1-ra)^2 + (2\pi n_g L)^2 ra\dfrac{(\lambda-\lambda_0)^2}{\lambda_0^4}}, \tag{1}$$

we obtain $a = 0.951$, $r = 0.964$, and an intrinsic loss per unit length of $\alpha_{int} = -20\log(a)/L = 3.47$ dB/cm. This corresponds to an intrinsic quality factor of $Q_{int} = 4.343\times 2\pi n_g/(\lambda_0\alpha_{int}) = 190{,}000$. We assume the observed Q_{ref} to be a result of both propagation loss and loss due to the through-port coupler, represented here by the coupler quality factor, Q_{coup}, where

$$\frac{1}{Q_{ref}} = \frac{1}{Q_{int}} + \frac{1}{Q_{coup}}. \tag{2}$$

The value of Q_{coup} is therefore 261,000, which corresponds to a coupler loss of $l_{coup} = 4.343\times 2\pi n_g L/(\lambda_0 Q_{coup}) = 0.32$ dB per pass in the resonator. The same value can be obtained from the Lorentzian fitting parameter r, where $l_{coup} = -20\log(r)$.

As shown in Fig. 3(a), the spectral response of the bare reference resonator was again measured with the waveguide sample heated to 100 °C using a substrate heater. The resonator quality factor was unaffected, which is expected since, even at 100 °C, free-carrier absorption is on the order of 10^{-2} dB/cm [20], and the propagation loss is dominated by scattering from the etched waveguide edges [21]. Furthermore, with a thermal expansion coefficient of just 2.6×10^{-6} °C $^{-1}$, the coupling gap and waveguide width change by a negligible amount for a temperature increase of 70 °C. However, due to the thermo-optic effect in the Si waveguide layer, the Si index changes by 5.2×10^{-5} °C $^{-1}$ [22]. This results in an increase of the modal effective index, n_{eff}, and the group index $n_g = n_{eff} - \lambda_0(\partial n_{eff}/\partial\lambda_0)$ with temperature, which redshifts each resonance by 0.08 nm/°C and slightly increases the FSR, as shown in Fig. 3.

#125843 - $15.00 USD Received 23 Mar 2010; revised 29 Apr 2010; accepted 4 May 2010; published 12 May 2010

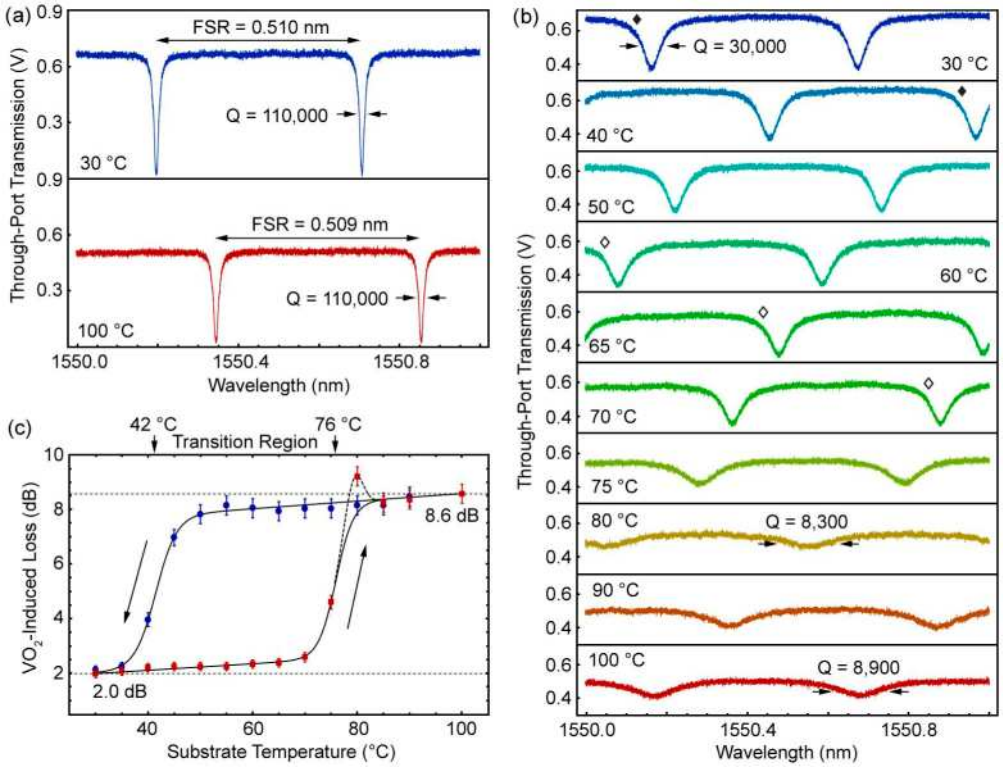

Fig. 3. (a) TE-polarized through-port transmission spectra of a critically coupled Si waveguide ring resonator without a VO_2 tab. The resonator Q is unchanged for substrate temperatures between 30 °C and 100 °C; however, grating coupling efficiency is impacted by the thermo-optic effect in Si, resulting in lower off-resonance transmission. (b) Through-port transmission spectra for increasing substrate temperature with the same resonator geometry, but with a 2 µm-long VO_2 tab. Modes of the same azimuthal order are indicated with diamond-shaped markers, revealing a thermally induced redshift of 0.08 nm/°C. (c) Round-trip resonator loss near 1550 nm due to the VO_2 tab. Upon cooling, thermal hysteresis of over 30 °C is observed.

We also observe that the off-resonance transmission for the reference devices is decreased when the sample is heated. Changes in the Si refractive index shift the ideal coupling angle of the grating couplers, resulting in decreased coupling efficiency of our devices when the angle is fixed. This illustrates the advantage of using resonator linewidth to probe attenuation: as long as the optical power is low enough that nonlinear effects are negligible, the linewidth provides an intensive measure of loss that is independent of coupled power. Consistent with the assumption of linearity, we measured no change in linewidth with input power for the laser intensities used here.

We then characterized ring resonators with VO_2 tabs patterned opposite the though-port coupler. Tabs with a 2-µm device length proved most conducive to the measurement technique employed here, as they were long enough to significantly perturb the ring resonator modes, but not so long as to absorb more light than is needed to reliably measure linewidth. The spectral response, shown in Fig. 3(b), was measured in the same manner as the reference resonator, and the substrate temperature was increased by 5 °C between measurements (for brevity, not all temperatures are shown in the figure). The sample was allowed to thermally stabilize for several minutes between measurements to eliminate transient effects in the VO_2. As expected based on the VO_2 refractive index, the presence of the tab significantly decreases the loaded quality factor, Q_{load}, of the TE resonator modes. Using the loaded quality factor of the otherwise identical reference resonator, Q_{ref}, we can isolate the effect of the tab by the relation

#125843 - $15.00 USD Received 23 Mar 2010; revised 29 Apr 2010; accepted 4 May 2010; published 12 May 2010

$$\frac{1}{Q_{load}} = \frac{1}{Q_{int}} + \frac{1}{Q_{coup}} + \frac{1}{Q_{tab}} = \frac{1}{Q_{ref}} + \frac{1}{Q_{tab}}. \quad (3)$$

The single-pass loss induced by the tab is therefore $l_{tab} = 4.343 \times 2\pi n_g L/(\lambda_0 Q_{tab})$, where n_g is unchanged from the reference resonator, as the tab length is just a small fraction of L.

At 30 °C, we observe Q_{load} = 30,000, and the quality factor decreases rapidly near the VO_2 phase transition temperature at 68 °C, ultimately falling to Q_{load} = 8,900 at 100 °C. These values of Q_{load} correspond to a modulator loss of 2.0 dB when the VO_2 is in its insulating phase and 8.6 dB for the metallic phase, as shown in Fig. 3(c), which is a 78% decrease in transmission. We define a modulator figure of merit (FOM) as the ratio of the modulation depth to the insulating-phase insertion loss, equal to 3.3 in this case.

At 80 °C, we also see a repeatable decrease in Q_{load} to 8,300, corresponding to a loss of over 9 dB. We attribute this seemingly anomalous increase in loss to a divergence of the real part of the index of VO_2, which was previously observed by Choi, *et al.* to be consistent with the percolation threshold of the insulator-to-metal transition [23]. During heating, isolated metallic domains are nucleated, and they become increasingly capacitively coupled as they expand toward one another. The net result, averaged over many crystal grains, is an increase in the effective dielectric constant. When the VO_2 is in its insulating phase, it is well index-matched to the Si index of 3.48, resulting in reasonable modal overlap with the VO_2 layer. According to Choi, *et al*., the VO_2 index in the infrared reaches approximately 4.5 just above the phase transition temperature, while the absorption is half of the bulk metallic-phase absorption. For our layered structure, this increase in index should pull the mode into the VO_2 layer, increasing the exposure of the mode to material absorption. As the phase transition progresses with increasing temperature, the VO_2 assumes metallic dielectric properties, and the mode is pushed further down into the transparent Si layer, as seen in Fig. 4(a).

We observe that as the sample is cooled from 100 °C, the VO_2 tab retains its metallic properties down to nearly 40 °C. As mentioned previously, such broad thermal hysteresis is characteristic of films with the large-grain microstructure observed here, where there is a relatively low density of nucleation sites for the metal-to-insulator transition. The width of the hysteresis loop matches our observations of electrical resistivity versus temperature, except that the onset of the metal-to-insulator transition during cooling is not as apparent in the optical measurements until the phase transition is nearly complete. During cooling, we also observe no anomalous increase in loss near the phase transition, suggesting that the nucleation of insulating domains in the VO_2 does not lead to isolation of metallic regions while the film still exhibits strongly metallic optical properties. We note that hysteresis can be undesirable in certain applications and could be reduced by preparing films with smaller crystal grains at lower temperatures [17], but broad hysteresis could be useful, for example, in optical memory devices.

Finally, as our SOI waveguides also support a TM mode, we attempted to characterize the VO_2-induced loss for TM modes in the devices described above. Interaction of TM resonator modes with the VO_2 tab was found to create additional spectral features that obfuscate the resonances. As a result, measurements of the linewidth were unreliable. These spectral features are likely due to substrate leakage, since the TM-mode is close to cutoff, as well as mode conversion to TE-polarized modes via scattering [15]. Nevertheless, as described in the next section, electromagnetic simulations show that TM-mode operation absent these effects still leads to inferior modulator performance compared with TE-mode operation.

5. Comparison with modeling

Figure 4(a) shows the optical power of the TE mode supported by our VO_2-clad waveguide geometry, as calculated using finite-element analysis (COMSOL). Assuming the insulating-phase dielectric properties of VO_2, 13.3% of the power lies in the modulator layer. For the metallic VO_2 layer, the optical mode is squeezed toward the Si/SiO_2 interface, resulting in a decreased real part of the modal effective index, n_{eff}. Although the power confinement in the VO_2 is reduced to 4.6% in the metallic phase, the 16-fold increase in absorption results in an

#125843 - $15.00 USD Received 23 Mar 2010; revised 29 Apr 2010; accepted 4 May 2010; published 12 May 2010

increase in the imaginary part of n_{eff} by a factor of 4.5. Assuming loss is due only to VO_2 absorption, we predict attenuation, in dB/cm, of $\alpha_{tab} = 4.343 \times 4\pi \, \mathrm{Im}[n_{eff}]/\lambda_0$. Over a 2-μm device length, the predicted losses for the insulating and metallic phases are therefore 1.8 dB and 7.9 dB, respectively. These values are each approximately 10% less than the measured losses for each phase of VO_2, suggesting that scattering from the VO_2 tab accounts for a small fraction of the loss, while material absorption is dominant.

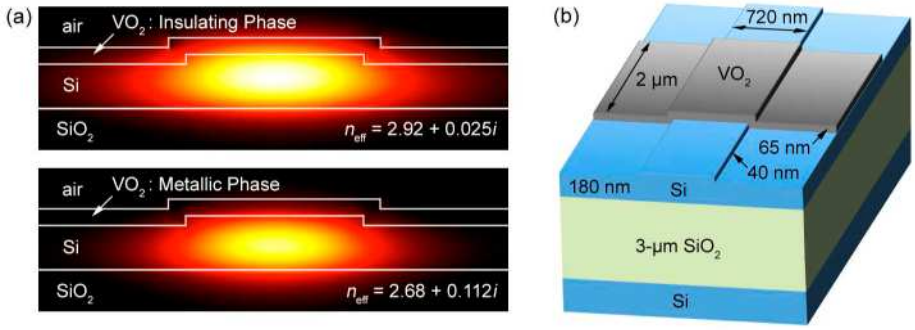

Fig. 4. (a) Power profiles of the fundamental TE mode in the VO_2-clad Si waveguide at 1550 nm, plotted over the same range of power. The imaginary part of the effective index, n_{eff}, indicates the substantially enhanced modal absorption in metallic-phase VO_2. (b) Schematic of the structure used in FDTD calculations, shown with the experimentally realized dimensions.

We also performed three-dimensional finite-difference time-domain (FDTD) calculations (Lumerical) with the waveguide structure shown in Fig. 4(b). Our idealized structure resembles the fabricated one except for the roughness of the polycrystalline VO_2; however, agreement of calculated loss with experiments further suggests that surface scattering is negligible compared with absorption. To obtain modulator loss with the FDTD simulations, we used the fundamental TE mode of the bare Si waveguide at 1550 nm as an input source and recorded the normalized reflected and transmitted power. The reflected power was found to be less than 0.2% for all tab geometries considered here, so excess loss beyond that due to VO_2 absorption is attributed to scattering into unguided modes. Consistent with the assertion that material loss is dominant for both VO_2 phases, loss increases linearly with device length, as seen in Fig. 5(a), and loss is minimal as the device length approaches zero. For a modulator with the experimental geometry, the insulating-phase loss is 2.1 dB and the metallic-phase loss is 8.2 dB, which agrees to within 5% of the measured values.

In Fig. 5(b), we show the calculated losses for a modulator layer of varying thickness. For VO_2 in its insulating phase, the loss per unit length scales linearly with VO_2 thickness, due to the increasing modal overlap of the fundamental TE mode with the VO_2 layer. For the metallic phase, the enhanced absorption leads to a sharp increase in loss versus thickness for thin VO_2 layers, but the loss saturates since the mode extends a limited distance into the layer. We find that the experimental thickness of 65 nm is almost exactly at the point where the metallic VO_2 layer completely extinguishes the mode on the topside of the modulator. Also plotted is the previously defined modulator FOM as a function of thickness, where we see the largest ratio of modulation depth to insulating-phase loss for a VO_2 thickness of just 5 nm. An 8 μm-long modulator with the indicated FOM would exhibit 15.0 dB loss in the metallic state and just 1.6 dB in the insulating state; however, our VO_2 deposition process cannot produce continuous films for such small layer thickness, as shown by Suh, *et al*. [17].

In the absence of clear loss measurements for the TM-polarized mode supported by our Si waveguides, we used FDTD to predict TM-mode modulator performance. The TM mode exhibits increased modal overlap with the VO_2 cladding since it is less confined in the Si layer, suggesting enhanced sensitivity to VO_2 index. Indeed, we calculate 16.8 dB loss for the experimental VO_2 tab geometry when the VO_2 is in its metallic state; however, the insulating-state loss is even further enhanced, resulting in 5.4 dB insertion loss. The corresponding modulator FOM is just 2.1, approximately two-thirds of the TE-mode FOM.

#125843 - $15.00 USD Received 23 Mar 2010; revised 29 Apr 2010; accepted 4 May 2010; published 12 May 2010

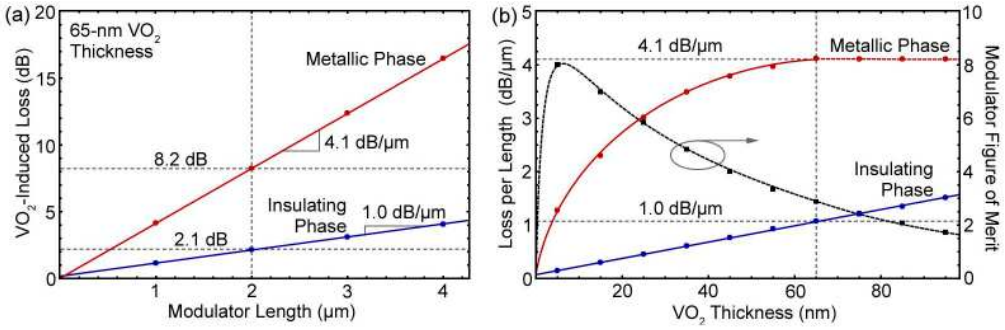

Fig. 5. (a) Simulated TE-mode loss due to a 65 nm-thick VO_2 tab as a function of tab length calculated using the three-dimensional FDTD method. The predicted losses for a 2-μm tab are within 5% of the measured values. (b) Simulated loss per unit length as a function of VO_2 film thickness. The dashed black curve is the modulator figure of merit, defined as the ratio of the modulation depth to the insertion loss.

6. Summary

We have demonstrated a compact VO_2-based absorption modulator at λ = 1550 nm on a Si waveguide platform as a potential component for future integrated optical circuits. While large-diameter ring resonators were used to accurately probe modulator loss, we show that in-line modulator devices need only be a few microns long, due to a measured 16-fold increase in material absorption at the VO_2 insulator-to-metal phase transition. By directly heating an integrated 2-μm device, we measured a single-pass loss of 2 dB at 30 °C, where VO_2 is in its insulating phase, and 8.6 dB at 100 °C, where VO_2 has transformed to its metallic phase, corresponding to a 78% decrease in transmission. We note that, as confirmed by electromagnetic simulations, simply extending the device length to 5 μm would result in modulation in excess of 16 dB, which is competitive with MZI and electro-absorption modulators, but the insertion loss in the insulating phase would be increased to 5 dB. Such a device was not quantitatively characterized with the ring-resonator test bed used here, as the large metallic-phase VO_2 loss almost completely extinguishes the cavity resonances; however, we envision that future devices will utilize more localized means to induce the phase transition, eliminating the need for a resonator as an accurate temperature-independent probe of modulation. In particular, since the VO_2 phase transition can also be induced athermally, future devices can potentially use local optical or electrical stimulus to not only induce the dramatic shift in absorption observed here, but do so on extremely short time scales.

Acknowledgements

The authors thank J.P.B. Müller for assistance with waveguide optimization and G.M. Kimball for valuable input on electrical measurements. This work was supported under AFOSR grant FA9550-06-1-0480. We gratefully acknowledge critical support and infrastructure provided by the Kavli Nanoscience Institute at Caltech. Portions of this work were also performed in facilities sponsored by the Center for Science and Engineering of Materials, an NSF MRSEC. R.M.B. acknowledges support from the National Defense Science and Engineering Graduate Fellowship, and I.M.P. acknowledges the support of the NSF Graduate Fellowship.

#125843 - $15.00 USD Received 23 Mar 2010; revised 29 Apr 2010; accepted 4 May 2010; published 12 May 2010